CGI-58 knockdown in mice causes hepatic steatosis but prevents diet-induced obesity and glucose intolerance[S]

J. Mark Brown,* Jenna L. Betters,* Caleb Lord,* Yinyan Ma,* Xianlin Han,† Kui Yang,† Heather M. Alger,§ John Melchior,* Janet Sawyer,* Ramesh Shah,* Martha D. Wilson,* Xiuli Liu, Mark J. Graham,†† Richard Lee,†† Rosanne Crooke,†† Gerald I. Shulman,§§ Bingzhong Xue,*** Hang Shi,††† and Liqing Yu[1],*,§**

Departments of Pathology Section on Lipid Sciences,* Biochemistry,§ Endocrinology and Metabolism,*** and Internal Medicine Section on Gerontology and Geriatric Medicine,††† Wake Forest University School of Medicine, Winston-Salem, NC 27157; Division of Bioorganic Chemistry and Molecular Pharmacology,† Department of Internal Medicine, Washington University School of Medicine, St. Louis, MO 63110; Department of Anatomic Pathology,** Cleveland Clinic, Cleveland, OH 44195; Cardiovascular Group,†† Antisense Drug Discovery, Isis Pharmaceuticals, Inc., Carlsbad, CA 92008-7208; and Departments of Internal Medicine and Cellular and Molecular Physiology,§§ Howard Hughes Medical Institute, Yale University School of Medicine, New Haven, CT 06510

Abstract Mutations of Comparative Gene Identification-58 (*CGI-58*) in humans cause triglyceride (TG) accumulation in multiple tissues. Mice genetically lacking CGI-58 die shortly after birth due to a skin barrier defect. To study the role of CGI-58 in integrated lipid and energy metabolism, we utilized antisense oligonucleotides (ASOs) to inhibit CGI-58 expression in adult mice. Treatment with two distinct CGI-58-targeting ASOs resulted in ~80–95% knockdown of CGI-58 protein expression in both liver and white adipose tissue. In chow-fed mice, ASO-mediated depletion of CGI-58 did not alter weight gain, plasma TG, or plasma glucose, yet raised hepatic TG levels ~4-fold. When challenged with a high-fat diet (HFD), CGI-58 ASO-treated mice were protected against diet-induced obesity, but their hepatic contents of TG, diacylglycerols, and ceramides were all elevated, and intriguingly, their hepatic phosphatidylglycerol content was increased by 10-fold. These hepatic lipid alterations were associated with significant decreases in hepatic TG hydrolase activity, hepatic lipoprotein-TG secretion, and plasma concentrations of ketones, nonesterified fatty acids, and insulin. Additionally, HFD-fed CGI-58 ASO-treated mice were more glucose tolerant and insulin sensitive. Collectively, this work demonstrates that CGI-58 plays a critical role in limiting hepatic steatosis and maintaining hepatic glycerophospholipid homeostasis and has unmasked an unexpected role for CGI-58 in promoting HFD-induced obesity and insulin resistance.—Brown, J. M., J. L. Betters, C. Lord, Y. Ma, X. Han, K. Yang, H. M. Alger, J. Melchior, J. Sawyer, R. Shah, M. D. Wilson, X. Liu, M. J. Graham, R. Lee, R. Crooke, G. I. Shulman, B. Xue, H. Shi, and L. Yu. **CGI-58 knockdown in mice causes hepatic steatosis but prevents diet-induced obesity and glucose intolerance. *J. Lipid Res.* 2010.** 51: **3306–3315.**

Supplementary key words fatty liver • insulin resistance • triglyceride hydrolysis • lipoprotein secretion • fatty acid oxidation

Neutral lipid storage disorder (NLSD) is a rare, nonlysosomal, autosomal recessive genetic disease characterized by the abnormal accumulation of triglyceride (TG) in

This work was supported in part by Intramural Grants from the Wake Forest University Health Sciences (to L.Y.), the Scientist Development Grant from the American Heart Association (to L.Y.), and the Award Number R01DK085176 (to L.Y.) from the National Institute of Diabetes and Digestive and Kidney Diseases. The content is solely the responsibility of the authors and does not necessarily represent the official views of the National Institute of Diabetes and Digestive and Kidney Diseases or the National Institutes of Health. The work was also supported in part by the Ruth L. Kirschstein National Research Service Award (NRSA) (1F32DK084582-01 to J.L.B.) provided by the National Institute of Diabetes and Digestive and Kidney Diseases and grants from the National Heart, Lung, and Blood Institute (1K99-HL096166-01 to J.M.B., 5P01HL049373-17 to J.S.P., and 5P01HL057278-09 to X.H.). All authors report that they have no conflicts of interest except X. Han, who has a financial relationship with LipoSpectrum LLC.

Manuscript received 2 August 2010 and in revised form 27 August 2010.

Published, JLR Papers in Press, August 27, 2010
DOI 10.1194/jlr.M010256

Abbreviations: ACC, acetyl CoA carboxylase; ASO, antisense oligonucleotide; ATGL, adipose triglyceride lipase; CDS, Chanarin-Dorfman syndrome; CGI-58, comparative gene identification 58; CE, cholesteryl ester; DGAT, acyl-CoA:diacylglycerol acyltransferase; FC, free cholesterol; GLUT, glucose transporter; GPAT, glycerol-3-phosphate acyltransferase; HFD, high-fat diet; HLM, hypotonic lysis medium; LCCoA, long-chain fatty acyl-CoA; LD, lipid droplet; LPAAT, lysophosphatidic acid acyltransferase; NEFA, nonesterified fatty acid; NLSD, neutral lipid storage disease; PA, phosphatidic acid; PG, phosphatidylglycerol; PL, phospholipid; PPAR, peroxisome proliferator-activated receptor; qPCR, quantitative real-time polymerase chain reaction; SCD, stearoyl-CoA desaturase; SREBP, sterol regulatory element binding protein; TG, triglyceride.

[1] To whom correspondence should be addressed.
e-mail: lyu@wfubmc.edu

[S] The online version of this article (available at http://www.jlr.org) contains supplementary data in the form of 13 figures.

multiple tissues including liver (1). All NLSD patients develop nonalcoholic fatty liver disease (1). A subset of patients with NLSD display thickened, scaly, dry skin known as ichthyosis (1). In the 1970s Chanarin et al. (2) and Dorfman et al. (3) reported some of these early cases and in recognition of their work, NLSD with ichthyosis was given the name Chanarin-Dorfman syndrome (CDS). In 2001, it was discovered that mutations in CGI-58 (also known as α/β hydrolase domain-containing protein-5, Abhd5) cause CDS (4). However, nearly a decade after the causal link between CGI-58 and CDS was established, we still do not completely understand how CGI-58 functions to prevent CDS.

Early studies using skin fibroblasts isolated from NLSD patients showed that these cultured cells had striking accumulation of intracellular TG, impaired turnover of long-chain fatty acids from stored TG (5, 6), and defective recycling of TG-derived acylglycerols into major phospholipid (PL) species (7–9). We and others have demonstrated that silencing of CGI-58 promotes TG stores by inhibiting intracellular TG hydrolysis in multiple cell types (10–15). However, CGI-58 itself does not posses intrinsic TG hydrolytic activity (13, 14), suggesting that CGI-58 has an indirect effect on TG hydrolysis. Recent in vitro evidence demonstrates that CGI-58 modulates TG hydrolysis by acting as a coactivator for adipose triglyceride lipase (ATGL) (14, 16, 17). In this case, it has been demonstrated that CGI-58 interacts directly with ATGL through a protein-protein interaction at the lipid droplet (LD) surface (14, 16). Importantly, in adipocytes, CGI-58 is associated with cytoplasmic LDs, achieving this subcellular localization by directly interacting with perilipin A (18, 19). In hepatoma cell models, CGI-58-driven TG hydrolysis is coupled to increased very low density lipoprotein (VLDL)-TG secretion and fatty acid β-oxidation (10, 15).

Although the prevailing theory is that CGI-58 regulates cellular TG content by serving as a coactivator of ATGL (14, 17, 20), there have been two in vitro studies showing that CGI-58 is an acyl-CoA-dependent lysophosphatidic acid acyltransferase (LPAAT) that prefers arachidonoyl-CoA and oleoyl-CoA as substrates (21, 22). Although the in vivo significance of this in vitro finding remains to be explored, CGI-58 mutations causing CDS were shown to have normal LPAAT activity (21), arguing against a role of defective LPAAT activity of CGI-58 in CDS development.

Collectively, cell-based and in vitro studies support a critical role of CGI-58 in controlling TG hydrolysis. Recently, total body CGI-58 knockout mice were generated (11). Unfortunately, these mice exhibit neonatal lethality due to a defective skin barrier function, making it difficult to study the role of CGI-58 in integrated lipid and energy metabolism. To circumvent this limitation we have utilized antisense oligonucleotides (ASOs) to inhibit the expression of CGI-58 in adult mice. Results from these studies demonstrate that CGI-58 limits hepatic steatosis by regulating hepatic TG and PL metabolism, and unexpectedly link CGI-58 to high-fat diet (HFD)-induced obesity and insulin resistance.

MATERIALS AND METHODS

Mice and ASO treatment

Male C57BL/6N mice were obtained from Harlan (Indianapolis, IN) at 3–4 weeks of age. At 8 weeks of age, mice were either maintained on standard rodent chow diet (Prolab RMH 3000) or switched to a synthetic HFD. The HFD was prepared by our institutional diet core and contains ~45% of energy as lard and ~0.015% (w/w) cholesterol. In conjunction with diet feeding, mice received biweekly intraperitoneal injections of either saline, a nontargeting control ASO (Control), or one of two independent ASOs targeting CGI-58 (CGI-58$^{\alpha}$; or CGI-58$^{\beta}$) for 8 weeks. The 20-mer phosphorothioate ASOs were designed to contain 2'-0-methoxyethyl groups at positions 1 to 5 and 15 to 20, and were synthesized, screened, and purified as described previously (23) by ISIS Pharmaceuticals (Carlsbad, CA). Following 8 weeks of dietary induction, all experimental animals were euthanized following a 4 h fast during the light cycle. Mice were maintained in a specific pathogen-free animal facility, and all experimental protocols were approved by the Institutional Animal Care and Use Committee at the Wake Forest University School of Medicine.

Plasma biochemistries

Unless otherwise stated, plasma samples were collected by submandibular vein puncture following a 4 h fast during the light cycle. For fasted and fed plasma samples, blood was collected by submandibular vein puncture at 9:00 AM in ad libitum fed mice (fed) or in mice fasted during the dark cycle for 12 h (9:00 PM–9:00 AM). Detailed description of plasma lipid and lipoprotein analyses has been previously described (24). Plasma β-hydroxybutyrate (Stanbio Laboratory, Boerne, TX), nonesterified fatty acids (NEFA-HR; Wako Diagnostics, Richmond, VA), aspartate aminotransferase, and alanine aminotransferase (Point Scientific, Inc. Canton, MI) were measured using commercially available kits. Plasma glucose levels were measured using a glucometer (Ascensia Countour, Bayer). Plasma insulin levels were measured by ELISA (Crystal Chem, Inc., Downers Grove, IL).

Immunoblotting

Tissue homogenates were made from multiple tissues in a modified RIPA buffer as previously described (24). Proteins (25 μg/lane) were separated by 4–12% SDS-PAGE, transferred to polyvinylidene difluoride membranes, and incubated with anti-CGI-58 mouse monoclonal (Novus Biologicals #HL00051099-M01), anti-Akt (Cell Signaling Technologies #2967), or anti-β-actin (Sigma #A5441).

Hepatic lipid analyses

Extraction of liver lipids and enzymatic quantification of total TG, cholesteryl esters (CEs), free cholesterol (FC), and PL were performed as previously described (24). Total liver NEFA was measured enzymatically (NEFA-HR; Wako Diagnostics) in detergent (1% Triton-X-100) solubilized liver extracts. Hepatic contents of diacylglycerol, ceramide, long-chain fatty acyl-CoA (LCCoA) and their molecular species were analyzed by liquid chromatography/tandem mass spectrometry as previously described (25, 26). Hepatic glycerophospholipid analyses were conducted using multi-dimensional mass spectrometry-based shotgun lipidomics as previously described (27, 28). Analyses were performed on a QqQ mass spectrometer (Thermo Fisher TSQ Quantum Ultra, San Jose, CA) equipped with an automated nanospray apparatus (i.e., Nanomate HD, Advion Bioscience Ltd., Ithaca, NY) and operated with an Xcalibur software system as previously described (29).

Determination of hepatic lipid secretion rates

The chow-fed mice underwent 4 weeks of ASO treatment. Recirculating isolated liver perfusions were performed in fed mice as previously described (30). During the 3 h of perfusion, a 1.5 ml aliquot of perfusate was removed every 30 min, and 1.5 ml of fresh medium containing erythrocytes was added back to the recirculation system. At the end of the 3 h period, all 10 ml of perfusate was collected. The final perfusate and all time point samples were centrifuged at 4°C to separate the medium from the erythrocytes. The lipids from each aliquot of perfusate were extracted, solubilized in 0.1% Triton X-100, and enzymatically quantified. Secretion rates of lipoprotein lipids, including TG, FC, and CE, were calculated using the amount of lipid in each time point sample. To adjust for one individual animal that was a true outlier, all secretion rate data were multiplied by a factor of 10 and then log transformed.

Measurement of TG hydrolase activity

TG hydrolase activity was measured according to the methods of Schweiger et al. (31) using a radiolabeled LD substrate isolated from HepG2 cells. To prepare LD-TG substrate, HepG2 cells were grown in DMEM with 10% FBS until ~70% confluent. Cells were treated with 2.5 μCi ^{3}H-9,10-oleic acid/ml + 0.8 mM cold oleic acid complexed to BSA for 16 h. LDs were isolated according to the published protocol (32). Cells were washed twice with ice-cold PBS and scraped in 5 ml ice-cold PBS/150 mm dish. The contents of two dishes were combined in one 15-ml Falcon tube and centrifuged (1,000 *g* at 4°C, 10 min). The supernatant was removed and the cells were resuspended in 1 ml ice-cold hypotonic lysis medium (HLM) (20 mM Tris-HCl, pH 7.4, 1 mM EDTA, 10 mM sodium fluoride, with protease inhibitor cocktail) with gentle pipetting. Resuspended cells were transferred to a Potter-Elvehjem tissue homogenizer and gently homogenized on ice. Homogenate was transferred to a clean 15 ml tube and centrifuged (1,000 *g* at 4°C, 10 min). The supernatant and floating fat layer were collected and adjusted to a final concentration of 20% sucrose in HLM. This was layered into a 13.2-ml ultracentrifuge tube and gently overlaid with 5 ml ice-cold HLM containing 5% sucrose. The remainder of the tube was filled with HLM and centrifuged 28,000 *g* at 4°C for 30 min using an SW41 rotor. LDs were collected as a white band from the top of the tubes and concentrated by centrifugation (20,000 *g* at 4°C, 15 min). The underlying solution was removed and LDs were resuspended in Buffer A (50 mM potassium phosphate, pH 7.4, 100 mM KCl, 1 mM EDTA, plus protease inhibitor cocktail) by brief sonication. TG content of LDs was determined using commercial reagents (Roche). Once LD substrate was prepared, livers were removed and washed in ice-cold PBS containing 2 U/ml heparin and 1 mM EDTA. Liver samples (~50 mg) were homogenized in Buffer B [20 mM Tris-HCl (pH 7.5), 0.25 M sucrose, 1 mM EDTA, 1 mM DTT, with protease inhibitor cocktail]. Cellular debris was removed by centrifugation (2,000 *g* at 4°C, 10 min). Tissue homogenate (100 μg) was incubated with 25 nmol ^{3}H-9,10-oleate labeled LD substrate and 5% defatted BSA in a total volume of 200 μl for 1 h in a 37°C water bath. Blank reactions contained no enzyme source. After incubation, the reaction was terminated by addition of 3.25 ml of methanol/chloroform/heptane (10:9:7) and 1 ml of 0.1 M potassium carbonate, 0.1 M boric acid, (pH 10.5). After centrifugation (800 *g*, 15 min), the release of FFA was determined by liquid scintillation counting of 1 ml of the upper phase.

qPCR

RNA extraction and quantitative real-time PCR (qPCR) was conducted as previously described (33) on pooled samples (n = 5 per group). Cyclophilin was used as an internal control. The mRNA level for each gene represents the amount relative to that in the control ASO-treated group, which was arbitrarily standardized to 1. Primers used for qPCR are available on request.

Glucose homeostasis

Intraperitoneal glucose tolerance tests and insulin tolerance tests were performed as previously described (24) in mice treated with diet and ASO for 6 or 7 weeks, respectively.

Statistical analysis

Data are expressed as the mean ± SEM. All data were analyzed using either a one-way or two-way ANOVA followed by Student's *t*-tests for post hoc analysis. All analyses were performed using JMP version 5.0.12 (SAS Institute; Cary, NC) software.

RESULTS

ASO-mediated knockdown of CGI-58 prevents HFD-induced obesity

CGI-58 serves as a coactivator for ATGL-mediated TG hydrolysis in vitro (14). ATGL knockout mice exhibit mild obesity (34). Given this, one would assume that CGI-58 deficiency would phenocopy the mild obesity seen in ATGL knockout mice. To examine this possibility, we treated adult mice with two distinct CGI-58-targeting ASOs, and this treatment resulted in ~80–95% knockdown of CGI-58 mRNA and protein expression in white adipose tissue and liver (**Figs. 1A**, B, **2A**, B). The most effective CGI-58 ASO, CGI-58$^{\beta}$, also caused substantial protein knockdown in brown adipose tissue (~50%), heart (~80%), skin (~70%), and spleen (~50%) (supplementary Fig. I). CGI-58$^{\alpha}$ ASO also knocked down CGI-58 protein expression in spleen by ~60% (supplementary Fig. I). In contrast, levels of CGI-58 were not affected by ASO treatment in brain, lung, or skeletal muscle (supplementary Fig. I). In chow-fed mice, CGI-58 knockdown did not significantly alter body weight (Fig. 1C), yet both CGI-58 ASOs promoted a ~50% decrease in epididymal fat pad weight compared with control mice (Fig. 1D). When challenged with a HFD, the saline and control ASO-treated mice gained in excess of 10 g in body weight over the 8 week feeding period, whereas mice treated with CGI-58 ASOs were completely resistant to HFD-induced obesity (Fig. 1C). In agreement, CGI-58 ASO-treated HFD-fed mice had a ~50% decrease in epididymal fat pad weight compared with control mice (Fig. 1D). Additionally, CGI-58 ASO-treated mice consumed the same amount of food over the 8 week feeding period (data not shown), likely indicating that CGI-58 ASO treatment promotes an increase in energy expenditure.

ASO-mediated knockdown of CGI-58 causes severe hepatic steatosis

Patients affected with CDS and CGI-58 knockout mice exhibit marked hepatic steatosis (1, 11). ASO treatment was extremely effective in diminishing the hepatic expression of CGI-58, with the CGI-58$^{\beta}$ ASO resulting in >98% knockdown at the mRNA and protein level (Fig. 2A, B). Knockdown of CGI-58 significantly decreased hepatic TG hydrolase activity on both diets (Fig. 2C), which was

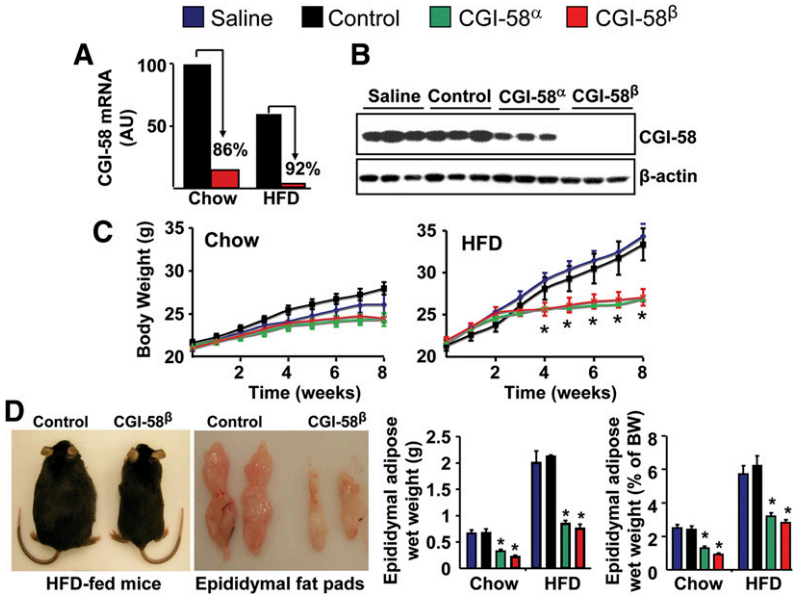

Fig. 1. ASO-mediated knockdown of CGI-58 prevents HFD-induced obesity. A: CGI-58 mRNA levels in the epididymal adipose tissue of mice treated with control ASO or CGI-58 ASO (CGI-58$^{\beta}$). B: Western blot analysis of epididymal adipose tissue in chow-fed mice (exposure time: 15 s). C: Body weight in ad libitum chow-fed or HFD-fed mice (n = 9–10). * $P < 0.01$ (vs. saline within each time point). D: Gross appearance of HFD-fed mice and their epididymal fat pads, and the total epididymal fat pad weight (g) and the total epididymal fat pad weight expressed as % of body weight (BW) in both chow-fed and HFD-fed mice (n = 9–10). * $P < 0.01$ (vs. saline or control ASO within each diet).

coupled to significantly reduced hepatic NEFA levels (Fig. 2D). In fact, in HFD-fed mice, hepatic NEFA levels were below levels of detection (Fig. 2D). Strikingly, CGI-58 ASO treatment caused severe hepatic steatosis in both chow-fed and HFD-fed mice (Fig. 2E, F). More specifically, CGI-58$^{\beta}$ ASO treatment in chow-fed mice resulted in steatosis composed predominantly of small vacuoles (microvesicular steatosis) and only occasional large fat vacuoles. Whereas HFD alone induced mild steatosis, CGI-58$^{\beta}$ ASO treatment in HFD-fed mice dramatically augmented hepatic fat

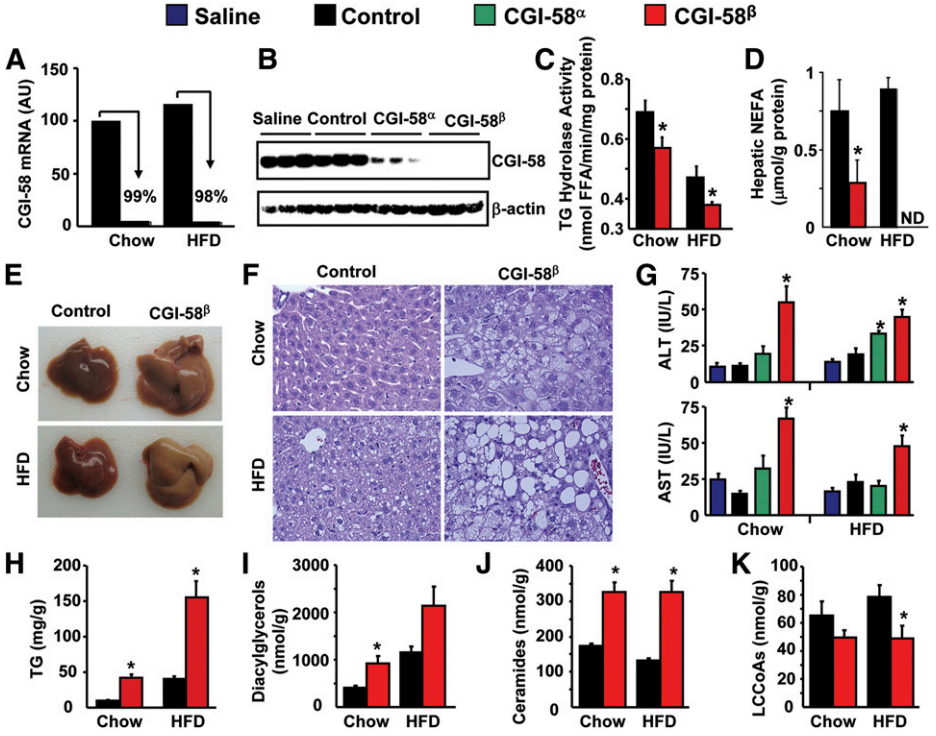

Fig. 2. ASO-mediated knockdown of CGI-58 causes severe hepatic steatosis. A: Hepatic CGI-58 mRNA expression in mice treated with control ASO or CGI-58 ASO (CGI-58$^{\beta}$). B: Western blot analysis of liver homogenates from chow-fed mice (exposure time: 30 s). C: Hepatic TG hydrolase activity (n = 6–7). * $P < 0.05$ (vs. control ASO within each diet). D: Hepatic NEFA levels (n = 8). * $P < 0.05$ (vs. control ASO in chow group). ND, not detectable. E: Liver appearance. F: Microscopic examination of liver sections (H and E staining, at 40× magnification). G: Plasma alanine aminotransferase (ALT) and aspartate aminotransferase (AST) levels (n = 6) *$P < 0.05$ (vs. saline or control ASO within each diet). H: Total hepatic TG levels (n = 8), *$P < 0.05$ (vs. control ASO within each diet). I–K: Total hepatic contents of diacylglycerol, ceramide, and LCCoA (n = 4–5). * $P < 0.05$ (vs. control ASO within each diet).

accumulation and resulted in severe steatosis composed of both small and large fat vacuoles (mixed macrovesicular and microvesicular steatosis). A modest (2- to 3-fold) elevation in plasma alanine aminotransferase and aspartate aminotransferase levels was associated with severe steatosis in both chow-fed CGI-58$^{\beta}$ ASO-treated mice and HFD-fed CGI-58$^{\beta}$ ASO-treated mice (Fig. 2G); however, no inflammatory infiltration or fibrosis was apparent on routine hematoxylin and eosin stained liver sections at this stage of disease under our dietary conditions. Regardless of diet, CGI-58 knockdown resulted in a 4-fold increase in total hepatic TG levels (Fig. 2H), but there were no differences in the fatty acid species of hepatic TG between control and CGI-58 ASO-treated mice (supplementary Fig. II). Interestingly, the chow-fed CGI-58 ASO-treated mice and the HFD-fed control ASO-treated mice had similar mass levels of hepatic TG (Fig. 2H), yet the morphology of the LDs within those respective livers was markedly different (Fig. 2F). CGI-58 knockdown also resulted in significantly elevated levels of hepatic diacylglycerols (Fig. 2I) and ceramides (Fig. 2J) with most molecular species of these complex lipids being elevated (supplementary Figs. III, IV). Consistent with reduced hepatic NEFA (Fig. 2D), total hepatic LCCoAs were significantly reduced by CGI-58 ASO treatment in HFD-fed mice (Fig. 2K) with significant reductions in monounsaturated (C16:1 and C18:1) LCCoAs (supplementary Fig. V). Collectively, these data demonstrate that CGI-58 knockdown promotes the hepatic accumulation of TG, diacylglycerols, and ceramides, while limiting the amount of hepatic NEFA and LCCoAs.

ASO-mediated knockdown of CGI-58 alters hepatic PL metabolism

Recent in vitro evidence suggests that CGI-58 is an acyl-CoA-dependent LPAAT (21, 22), but the importance of CGI-58 in maintaining PL homeostasis in vivo has never been reported. We found that CGI-58 knockdown did not alter total PL levels in chow-fed mice but significantly increased total hepatic PL levels in HFD-fed mice (**Fig. 3A**). Importantly, CGI-58 ASO treatment in HFD-fed mice did not alter total hepatic PA levels but did result in a significant increase in 18:0/18:1 PA (Fig. 3C). In addition, CGI-58 knockdown resulted in significantly reduced levels of total hepatic phosphatidylcholine (Fig. 3D), with some molecular species of phosphatidylcholine being decreased and some being increased with CGI-58 ASO treatment (supplementary Fig. VI). Likewise, knockdown of CGI-58 caused significant reductions in total hepatic phosphatidylethanolamine levels (Fig. 3E) with an interesting pattern of acyl-chain specificity (supplementary Fig. VII). In contrast, CGI-58 did not alter total hepatic phosphatidylserine levels (Fig. 3F), yet did cause a significant increase in 18:0/22:5 and 18:0/22:4 phosphatidylserine species (supplementary Fig. VIII). CGI-58 knockdown also promoted a significant increase in total hepatic sphingomyelin levels (Fig. 3G), with the majority of the increase coming from N16:0 and N24:1 sphingomyelin species (supplementary Fig. IX). The most striking effect of CGI-58 knockdown on hepatic PL was apparent in phosphatidylglycerol (PG) species. CGI-58 knockdown caused a 10-fold increase in total hepatic PG levels (Fig. 3H), with the majority of this increase being in atypical hepatic PG species (i.e., species other than palmitoyl-oleoyl-PG, POPG) (supplementary Fig. X). PG is usually a precursor for the synthesis of cardiolipin. Although CGI-58 ASO treatment did not significantly alter the total hepatic level of cardiolipin (Fig. 3I), it actually decreased the major species of hepatic cardiolipin (supplementary Fig. XI). Collectively, these in vivo data support a critical role of CGI-58 in maintaining normal hepatic PL homeostasis.

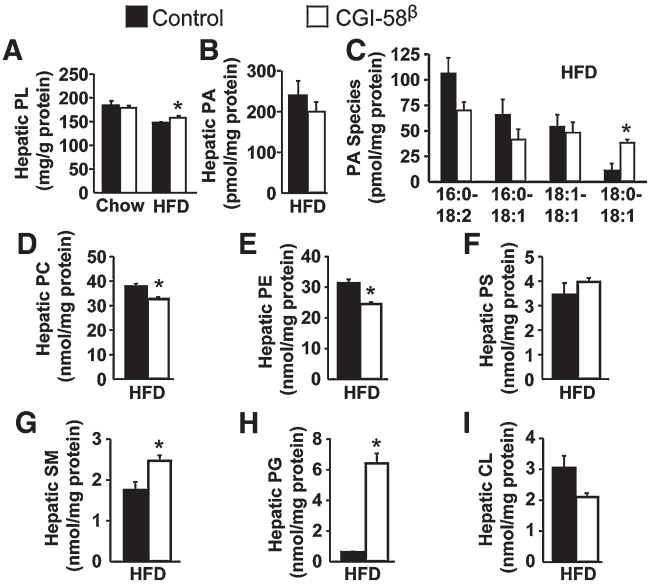

Fig. 3. ASO-mediated knockdown of CGI-58 alters hepatic phospholipid metabolism. A: Total hepatic PL levels (n = 8). * $P < 0.05$ (vs. control ASO within each diet). B–G: Hepatic contents of total PA, PA species, total phosphatidylcholine (PC), total phosphatidylethanolamine (PE), total phosphatidylserine (PS), and total sphingomyelin (SM) in HFD-fed mice (n = 4). * $P < 0.05$ (vs. control ASO). H: Total hepatic PG levels in HFD-fed mice (n = 4). * $P < 0.01$ (vs. control ASO). I: Total hepatic cardiolipin (CL) levels in HFD-fed mice (n = 4).

CGI-58 regulates hepatic lipid secretion and fasting-induced ketogenesis

We have previously demonstrated that CGI-58-driven TG hydrolysis is critical for promoting both VLDL-TG secretion and fatty acid β-oxidation in hepatoma cells (10). To investigate the role of CGI-58 in VLDL-TG secretion in vivo, we performed isolated recirculating liver perfusions and determined the hepatic secretion rates of TG, CE, and FC. ASO-mediated knockdown of CGI-58 resulted in a significant reduction in the hepatic secretion rates for both TG and CE yet hepatic FC secretion was not affected by CGI-58 knockdown (**Fig. 4A**). Interestingly, CGI-58 knockdown did not alter plasma TG levels in chow-fed mice (supplementary Fig. II) and only modestly decreased postprandial plasma TG levels in HFD-fed mice (Fig. 4B). CGI-58 ASO treatment significantly elevated total plasma cholesterol (TPC), low density lipoprotein cholesterol, and high density lipoprotein cholesterol in chow-fed mice (supplementary Figs. XII, XIII), but did not alter plasma

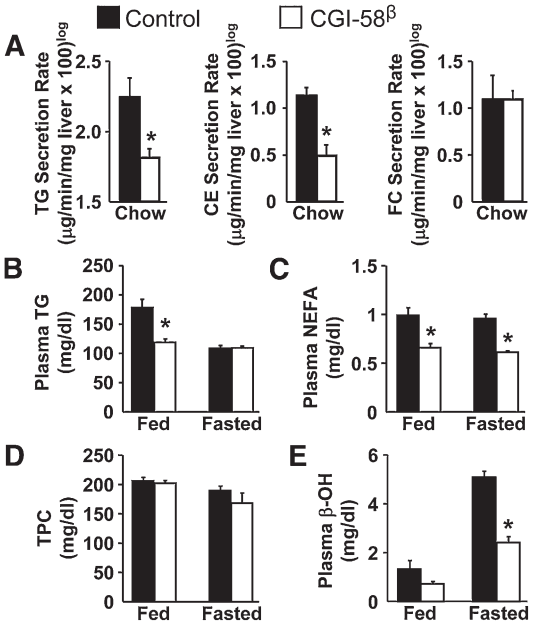

Fig. 4. CGI-58 regulates plasma lipid metabolism and fasting-induced ketogenesis. At 8 weeks of age, male C57BL/6N mice were either maintained on standard chow (A) or switched to a HFD (B–E) in conjunction with biweekly injections of ASOs for 4 weeks. A: Hepatic secretion rates of TG, CE, and FC determined by recirculating isolated liver perfusion in fed mice (n = 4–5). * $P < 0.05$. B: Plasma concentrations of TG levels (n = 8). * $P < 0.05$ (vs. control ASO within each dietary condition). C: Plasma NEFA levels (n = 8). * $P < 0.01$ (vs. control ASO group within each dietary condition). D: Total plasma cholesterol (TPC) levels (n = 8). E: Plasma β-hydroxybutyrate (β-OH) levels (n = 8). * $P < 0.01$ (vs. control ASO group within each dietary condition).

cholesterol levels in HFD-fed mice (Fig. 4D). CGI-58 knockdown in chow-fed mice did not significantly alter fed or fasting plasma NEFA levels (supplementary Fig. XII), but caused a ~35% decrease in plasma NEFA levels in both the fed and fasted (12 h) state in HFD-fed mice (Fig. 4C). Furthermore, the levels of plasma β-hydroxybutyrate following a 12 h fast were reduced by 53% in HFD-fed mice treated with CGI-58 ASO (Fig. 4E).

CGI-58 ASO-treated mice are protected against HFD-induced insulin resistance

Given the striking hepatic steatosis seen with CGI-58 ASO treatment (Fig. 2), we anticipated that mice with CGI-58 knockdown would present with hepatic insulin resistance. To our surprise, CGI-58 ASO treatment actually prevented HFD-induced hyperglycemia (**Fig. 5A**). In HFD-fed mice, CGI-58 knockdown significantly reduced plasma insulin levels in both the fed and fasted state (Fig. 5B). Furthermore, mice treated with CGI-58 ASOs had improved glucose tolerance when fed a chow diet, and were completely protected against HFD-induced glucose intolerance (Fig. 5C). During glucose tolerance tests, plasma insulin levels were markedly lower in CGI-58 ASO-treated mice at all time points (Fig. 5D). When intraperitoneal insulin tolerance tests were performed, it was found that CGI-58 knockdown protected against HFD-induced systemic insulin resistance (Fig. 5E).

CGI-58 knockdown alters gene expression in liver and white adipose tissue

To gain insights into the molecular basis of hepatic steatosis and obesity prevention driven by CGI-58 ASO treatment, we used pooled RNA samples and measured the mRNA abundance of key enzymes in TG, fatty acid, and glucose metabolism in liver and white fat, two tissues showing the most dramatic knockdown of CGI-58 expression after ASO injections (Figs. 1, 2).The pooled RNA samples (n = 5 in each group) were chosen because we wanted to screen as many genes in the same metabolic pathway as possible. The pooled RNA samples have been used to show consistent changes (in the same direction) of key genes in a given metabolic or signaling pathway and these changes have been demonstrated to be physiologically relevant (33, 35–38).

In the liver, CGI-58 knockdown by CGI-58$^{\beta}$ ASO in chow-fed mice resulted in a substantial decrease in the expression of all lipogenic genes examined, including sterol regulatory element binding protein 1c (SREBP-1c), fatty acid synthase (FAS), acetyl CoA carboxylase 1 (ACC1), stearoly-CoA desaturase 1 (SCD-1), malic enzyme (ME), mitochondrial glycerol-3-phosphate acyltransferase (GPAT), and acyl-CoA:diacylglycerol acyltransferase 2 (DGAT2) (**Table 1**). Furthermore, CGI-58 ASO treatment prevented HFD-induced upregulation of these same lipogenic genes (Table 1). This observation indicates that hepatic steatosis induced by CGI-58 knockdown was unlikely a result of increased lipogenesis.

Consistently with reduced plasma β-hydroxybutyrate concentrations in CGI-58 ASO-treated mice (Fig. 4E), genes involved in fatty acid catabolism and ketogenesis (i.e., fatty acid transport protein 1 or FATP1; peroxisome proliferator-activated receptor α or PPARα; acyl-CoA oxidase or ACO; long-chain acyl-CoA dehydrogenase or LCAD; and mitochondrial HMG-CoA synthase 2 or HMGCS2) were also reduced by CGI-58 ASO treatment regardless of diet (Table 1). In contrast, PPARγ target genes (adipocyte fatty acid binding protein or aP2; cluster determinate 36 or CD36) were higher in the livers of CGI-58 ASO treated mice (Table 1).

Additionally, the hepatic expression of several genes involved in gluconeogenesis and insulin signaling (glucokinase or GK; phosphoenolpyruvate-carboxykinase or PEPCK; glucose-6-phosphatase or G-6-P; insulin receptor substrate 2 or IRS-2) were diminished by CGI-58 ASO treatment, particularly in HFD-fed mice (Table 1).

In the epididymal fat, CGI-58 knockdown by CGI-58$^{\beta}$ ASO reduced the abundance of mRNAs for the lipolytic enzymes ATGL and lipoprotein lipase (LPL), lipogenic proteins SCD-1, FAS, and SREBP-1c, and the glucose transporter 4 (GLUT4) in both chow- and HFD-fed mice (**Table 2**). Compared with chow diet, HFD appeared to inhibit the expression of all of these genes in the epididymal fat (Table 2).

These data together suggest that substantial transcriptional reprogramming occurs in the liver and white adipose tissue under conditions where CGI-58 levels are diminished. Considering that CGI-58 knockdown reduced TG hydrolase

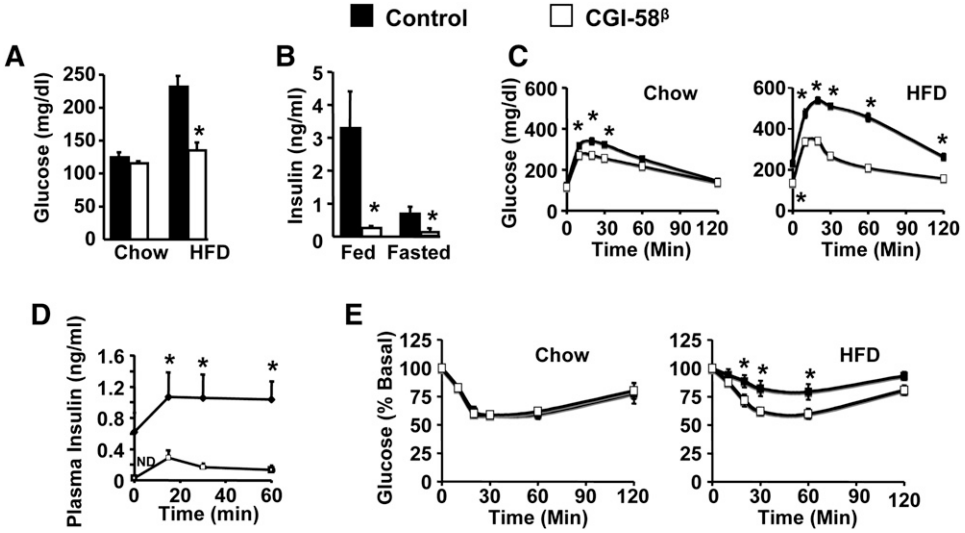

Fig. 5. CGI-58 ASO-treated mice are protected against HFD-induced insulin resistance. A: Fasting plasma glucose levels (n = 6). * $P < 0.05$ (vs. control ASO within each diet). B: Fed and fasting plasma insulin levels in HFD-fed mice (n = 8). * $P < 0.05$ (vs. control ASO within each dietary condition). C: Glucose tolerance tests (n = 8). * $P < 0.01$ (vs. control ASO within each time point). D: Plasma insulin levels during glucose tolerance tests (n = 6). * $P < 0.01$ (vs. control ASO within each time point). E: Insulin tolerance tests (n = 8). * $P < 0.01$ (vs. control ASO within each time point).

activity (Fig. 2C), our data may also suggest a feedback suppression of de novo lipogenesis when TG hydrolysis is inhibited in both liver and white adipose tissue, two important lipogenic tissues. Attenuated lipogenesis in the white adipose tissue may in part explain why mice treated with CGI-58 ASOs are resistant to HFD-induced obesity.

DISCUSSION

To our knowledge, this is the first study to document the role of CGI-58 in regulating integrative lipid and glucose metabolism in adult mice. The major findings of this work demonstrate that ASO-mediated knockdown of CGI-58: *1*) prevents HFD-induced obesity and even reduces the epididymal fat pad weight in chow-fed mice, *2*) promotes hepatic accumulation of TG, diacylglycerols, and ceramides, *3*) alters hepatic glycerophospholipid metabolism, *4*) diminishes hepatic contents of NEFA and LCCoAs, *5*) decreases hepatic secretion of VLDL-TG and VLDL-CE, *6*) blunts fasting-induced ketogenesis, and *7*) prevents HFD-induced systemic insulin resistance.

CGI-58 interacts with ATGL to augment in vitro TG hydrolase activity of ATGL (12, 14, 16, 17, 39). Liver expresses several TG hydrolases including ATGL. Although CGI-58's lipase targets in the liver remain to be identified, CGI-58 knockdown significantly reduces hepatic TG hydrolase activity (Fig. 2C), which can at least partly explain increased hepatic TG accumulation (Fig. 2H). It is unlikely that hepatic steatosis seen in CGI-58 ASO-treated mice results from increased de novo lipogenesis because hepatic expression levels of all the lipogenic genes examined were substantially lower in these animals (Table 1). Perhaps TG hydrolysis inhibition is sensed by cells, generating signals capable of inhibiting expression of genes related to fatty acid and TG synthesis.

During TG hydrolysis, TG is first converted to diacylglycerols. Inhibiting CGI-58-driven TG hydrolysis may reduce the cellular diacylglycerol pool. However, the opposite was found in CGI-58 ASO-treated mice (Fig. 2I). Diacylglycerol can be hydrolyzed to monoacylglycerols by other lipases, synthesized from and recycled to PL, or reesterified to TG. It is unclear if CGI-58 modulates hepatic diacylglycerol hydrolase activity, but it was shown that the recycling of acylglycerols to PL is defective in fibroblasts obtained from one CDS patient (8). We found that the hepatic mRNA level of acyl-CoA:diacylglycerol acyltransferase 2, an enzyme critical in diacylglycerol acylation to TG, is ~50% lower in CGI-58 ASO-treated mice compared with controls (Table 1). Therefore, CGI-58 inhibition may cause hepatic diacylglycerol accumulation by collectively influencing all these metabolic pathways directly or indirectly. Alternatively, elevated hepatic diacylglycerols and perhaps ceramides may be attributable to simple sequestration of these lipids in cytosolic LDs accumulated in the CGI-58 knockdown liver (Fig. 2F).

CGI-58 has an intrinsic LPAAT activity, capable of converting lysophosphatidic acid to PA in vitro (21, 22). PA can be used as a precursor for the synthesis of acylglycerols and phospholipids. However, CGI-58-derived PA is unlikely used directly for, or to significantly contribute to, acylglycerol synthesis because inhibiting CGI-58 increases, rather than reduces, cellular TG and diacylglycerol levels. Interestingly, ASO-mediated knockdown of CGI-58 in mice raises the hepatic PG content by ~10-fold in HFD-fed mice (Fig. 3H). Future studies are required to define how PG is accumulated in the liver of CGI-58 ASO-treated mice and whether PG accumulation is a common feature of fatty liver induced by TG hydrolysis inhibition. Additionally, PG is the precursor of cardiolipin and both lipids are enriched in mitochondria (40). Some PG species have anti-inflammatory

TABLE 1. Relative hepatic mRNA levels

	Chow		HFD	
	Con. ASO	CGI ASO	Con. ASO	CGI ASO
Lipogenesis				
SREBP-1c	1	0.69	1.18	0.53
FAS	1	0.63	2.71	0.66
ACC1	1	0.67	1.71	0.62
SCD-1	1	0.42	3.07	0.65
ME	1	0.31	2.03	0.26
GPAT	1	0.42	1.91	0.8
DGAT2	1	0.55	1.19	0.46
Fatty acid transport and oxidation				
FATP-1	1	0.54	0.9	0.5
PPAR-α	1	0.8	1.37	0.61
PGC-1α	1	2.06	1.59	1.14
CPT-1α	1	1.04	1.15	0.65
ACO	1	0.58	1.25	0.53
LCAD	1	0.85	1.4	0.73
HMGCS2	1	0.55	1.26	0.48
FGF21	1	0.68	0.14	0.96
PPAR-γ and its targets				
PPAR-γ	1	0.82	1.07	1.17
aP2	1	1.99	1.09	2.45
CD36	1	1.88	1.64	2.51
Glucose metabolism and insulin signaling				
GK	1	0.97	1.85	0.91
PEPCK	1	0.9	1.06	0.47
G6P	1	0.61	1.39	0.25
GLUT2	1	0.65	1.23	0.58
ChREBP	1	0.61	0.88	0.4
FOXO1	1	0.54	1.11	0.74
IRS2	1	0.64	0.48	0.53
Cholesterol synthesis				
SREBP-2	1	0.74	0.85	0.36
HMGCS	1	0.55	0.79	0.22
HMGCR	1	1.21	1.24	0.9
Triglyceride hydrolysis				
CGI-58	1	0.01	1.16	0.02
ATGL	1	1.59	0.9	0.71

Liver tissues were collected from male C57BL/6 mice treated with control (Con.) ASO or CGI-58$^{\beta}$ ASO (CGI ASO) for 8 weeks and the total RNA was extracted from individual liver samples. An equal amount of total RNA from each sample in each group (n = 5) was pooled and subjected to qPCR as described in Materials and Methods. LCAD, long-chain acyl-CoA dehydrogenase; ME, malic enzyme.

properties (41). In the future, it would be interesting to determine if CGI-58 inhibition influences fatty liver development and energy metabolism by modulating mitochondrial function and inflammatory signaling.

It was previously demonstrated that CGI-58-driven TG hydrolysis is critical for VLDL-TG secretion in hepatoma cells (10, 15). The in vivo knockdown of CGI-58 with ASOs confirms these cell-based findings (Fig. 4A). It is likely that CGI-58-mediated TG hydrolysis simply provides the necessary cytosolic NEFA and acylglycerol substrates for subsequent reesterification in the endoplasmic reticulum for incorporation into VLDL particles, but it remains possible that CGI-58 plays other roles in VLDL assembly. We have also previously demonstrated that CGI-58-driven TG hydrolysis is coupled in increased fatty acid oxidation in cultured cells (10). Although we did not directly measure fatty acid oxidation in these studies, CGI-58 knockdown did result in diminished fasting-induced ketogenesis (Fig. 4E), which is primarily driven by β-oxidation in the liver. In this case, it is reasonable to assume that CGI-58-mediated TG hydrolysis simply provides the necessary NEFA substrate for subsequent conversion into ketone bodies in the liver. However, it is also important to note a number of PPARα target genes were downregulated with CGI-58 knockdown in the liver (Table 1). PPARα is a well-known master regulator of fatty acid oxidation and ketogenesis in the liver. Therefore, it is tempting to speculate that CGI-58-driven TG hydrolysis may liberate endogenous PPARα ligand(s) from the cytosolic LD. Nonetheless, reduced hepatic VLDL-TG secretion and fatty acid oxidation may in turn exacerbate hepatic steatosis in CGI-58 ASO-treated mice.

TABLE 2. Relative mRNA levels in white adipose tissue

	Chow		HFD	
	Con. ASO	CGI ASO	Con. ASO	CGI ASO
CGI-58	1	0.14	0.6	0.05
ATGL	1	0.46	0.46	0.4
LPL	1	0.34	0.67	0.18
SCD-1	1	0.24	0.67	0.18
FAS	1	0.16	0.52	0.04
SREBP-1c	1	0.39	0.4	0.21
GLUT4	1	0.3	0.39	0.14

Epididymal fat tissues were collected from male C57BL/6 mice treated with control (Con.) ASO or CGI-58$^{\beta}$ ASO (CGI ASO) for 8 weeks and the total RNA was extracted from individual fat samples. An equal amount of total RNA from each sample in each group (n = 5) was pooled and subjected to qPCR as described in Materials and Methods.

If CGI-58's sole function is to coactivate ATGL, one would assume that CGI-58 knockdown promotes weight gain by inhibiting fat lipolysis because ATGL knockout mice exhibit mild obesity (34). But the opposite was found and ASO-mediated knockdown of CGI-58 actually prevents HFD-induced obesity and even reduces the epididymal fat pad weight in chow-fed mice (Fig. 1). In humans, mutations in CGI-58 cause TG accumulation in most tissues but fat (ectopic fat deposition) (1). Thus, our observation in CGI-58 ASO-treated mice is consistent with findings in human CDS patients. It is difficult to measure the white adipose tissue weight in the whole-body CGI-58 knockout mice because these animals die within 16 h after birth (11). The systemic fat accumulation found in the carcass of these neonates may mainly be attributable to fat deposition in nonadipose tissues such as liver and skin (11). Nonetheless, our observation suggests that although one function of CGI-58 is to coactivate ATGL, there are likely ATGL-independent functions of CGI-58 that need to be further explored. For instance, CGI-58 was shown to activate lipases distinct from ATGL in skin (11). Thus, CGI-58 may have distinctive lipase targets in different tissues. In addition, the mRNA levels of genes related to TG hydrolysis, lipogenesis, and glucose transport are substantially lower in the white fat of mice treated with CGI-58 ASO (Table 2), implying that CGI-58 ASO-treated mice may have a defect in diet-induced adipogenesis. Furthermore, CGI-58 knockdown in mice may protect against diet-induced weight gain by increasing energy expenditure because the food intake was not altered (data not shown). Future studies should focus on metabolic phenotyping of CGI-58 knockdown animals.

Hepatic steatosis is often accompanied by insulin resistance. In HFD-fed CGI-58 ASO-treated mice, however, despite severe hepatosteatosis, systemic insulin sensitivity is significantly higher. Although this may be attributable to reduced weight gain in these animals, the ultimate mechanism by which CGI-58 knockdown protects against HFD-induced insulin resistance is still elusive. In CGI-58 ASO-treated mice, the hepatic diacylglycerol content was increased (Fig. 2I), and it has been previously demonstrated that elevated hepatic diacylglycerol levels contribute to HFD- and obesity-linked insulin resistance (25, 26, 42–46). Thus the improved systemic insulin sensitivity seen in CGI-58 ASO-treated mice may be largely attributable to metabolic alterations in non-hepatic tissues. Given that CGI-58 modulates TG hydrolysis and glycerophopholipid metabolism (Fig. 4) (21, 22), it is also tempting to speculate that CGI-58 knockdown may improve insulin sensitivity by inhibiting generation of signaling-competent lipotoxic lipids from cytosolic LDs (47). Alternatively, CGI-58 inhibition may improve insulin sensitivity by causing sequestration of insulin signaling-suppressing lipids in cytosolic LDs away from the insulin signaling regulatory pool. This lipid compartmentalization may also explain why not all subjects or animals with hepatic steatosis develop insulin resistance. Perhaps how and where insulin signaling-suppressing lipids are accumulated is more important than the total cellular lipids in determining insulin sensitivity.

In summary, we have demonstrated that ASO-mediated knockdown of CGI-58 results in marked hepatic accumulation of TG, diacylglycerols, and ceramides, yet protects mice from HFD-induced obesity and systemic insulin resistance. Further investigation into the underlying molecular mechanisms should provide novel mechanistic insights into the causal relationship between lipid metabolism and insulin resistance. Given CGI-58's ubiquitous expression pattern (10) and total body knockouts die prematurely (11), tissue-specific knockouts will be required for these mechanistic studies in this complicated metabolic phenotype.

REFERENCES

1. Igal, R. A., J. M. Rhoads, and R. A. Coleman. 1997. Neutral lipid storage disease with fatty liver and cholestasis. *J. Pediatr. Gastroenterol. Nutr.* **25:** 541–547.
2. Chanarin, I., A. Patel, G. Slavin, E. J. Wills, T. M. Andrews, and G. Stewart. 1975. Neutral-lipid storage disease: a new disorder of lipid metabolism. *BMJ.* **1:** 553–555.
3. Dorfman, M. L., C. Hershko, S. Eisenberg, and F. Sagher. 1974. Ichthyosiform dermatosis with systemic lipidosis. *Arch. Dermatol.* **110:** 261–266.
4. Lefevre, C., F. Jobard, F. Caux, B. Bouadjar, A. Karaduman, R. Heilig, H. Lakhdar, A. Wollenberg, J. L. Verret, J. Weissenbach, et al. 2001. Mutations in CGI-58, the gene encoding a new protein of the esterase/lipase/thioesterase subfamily, in Chanarin-Dorfman syndrome. *Am. J. Hum. Genet.* **69:** 1002–1012.
5. Hilaire, N., A. Negre-Salvayre, and R. Salvayre. 1993. Cytoplasmic triacylglycerols and cholesteryl esters are degraded in two separate catabolic pools in cultured human fibroblasts. *FEBS Lett.* **328:** 230–234.
6. Hilaire, N., R. Salvayre, J. C. Thiers, M. J. Bonnafe, and A. Negre-Salvayre. 1995. The turnover of cytoplasmic triacylglycerols in human fibroblasts involves two separate acyl chain length-dependent degradation pathways. *J. Biol. Chem.* **270:** 27027–27034.
7. Williams, M. L., R. A. Coleman, D. Placezk, and C. Grunfeld. 1991. Neutral lipid storage disease: a possible functional defect in phospholipid- linked triacylglycerol metabolism. *Biochim. Biophys. Acta.* **1096:** 162–169.
8. Igal, R. A., and R. A. Coleman. 1996. Acylglycerol recycling from triacylglycerol to phospholipid, not lipase activity, is defective in neutral lipid storage disease fibroblasts. *J. Biol. Chem.* **271:** 16644–16651.
9. Igal, R. A., and R. A. Coleman. 1998. Neutral lipid storage disease: a genetic disorder with abnormalities in the regulation of phospholipid metabolism. *J. Lipid Res.* **39:** 31–43.
10. Brown, J. M., S. Chung, A. Das, G. S. Shelness, L. L. Rudel, and L. Yu. 2007. CGI-58 facilitates the mobilization of cytoplasmic triglyceride for lipoprotein secretion in hepatoma cells. *J. Lipid Res.* **48:** 2295–2305.
11. Radner, F. P., I. E. Streith, G. Schoiswohl, M. Schweiger, M. Kumari, T. O. Eichmann, G. Rechberger, H. C. Koefeler, S. Eder, S. Schauer, et al. 2010. Growth retardation, impaired triacylglycerol catabolism, hepatic steatosis, and lethal skin barrier defect in mice lacking comparative gene identification-58 (CGI-58). *J. Biol. Chem.* **285:** 7300–7311.
12. Bezaire, V., A. Mairal, C. Ribet, C. Lefort, A. Girousse, J. Jocken, J. Laurencikiene, R. Anesia, A. M. Rodriguez, M. Ryden, et al. 2009. Contribution of adipose triglyceride lipase and hormone-sensitive lipase to lipolysis in hMADS adipocytes. *J. Biol. Chem.* **284:** 18282–18291.
13. Yamaguchi, T., N. Omatsu, E. Morimoto, H. Nakashima, K. Ueno, T. Tanaka, K. Satouchi, F. Hirose, and T. Osumi. 2007. CGI-58 facilitates lipolysis on lipid droplets but is not involved in the vesiculation of lipid droplets caused by hormonal stimulation. *J. Lipid Res.* **48:** 1078–1089.
14. Lass, A., R. Zimmermann, G. Haemmerle, M. Riederer, G. Schoiswohl, M. Schweiger, P. Kienesberger, J. G. Strauss, G. Gorkiewicz, and R. Zechner. 2006. Adipose triglyceride lipase-mediated lipolysis of cellular fat stores is activated by CGI-58 and defective in Chanarin-Dorfman Syndrome. *Cell Metab.* **3:** 309–319.

15. Caviglia, J. M., J. D. Sparks, N. Toraskar, A. M. Brinker, T. C. Yin, J. L. Dixon, and D. L. Brasaemle. 2009. ABHD5/CGI-58 facilitates the assembly and secretion of apolipoprotein B lipoproteins by McA RH7777 rat hepatoma cells. *Biochim. Biophys. Acta.* **1791:** 198–205.
16. Granneman, J. G., H. P. Moore, R. L. Granneman, A. S. Greenberg, M. S. Obin, and Z. Zhu. 2007. Analysis of lipolytic protein trafficking and interactions in adipocytes. *J. Biol. Chem.* **282:** 5726–5735.
17. Granneman, J. G., H. P. Moore, R. Krishnamoorthy, and M. Rathod. 2009. Perilipin controls lipolysis by regulating the interactions of AB-hydrolase containing 5 (Abhd5) and adipose triglyceride lipase (Atgl). *J. Biol. Chem.* **284:** 34538–34544.
18. Subramanian, V., A. Rothenberg, C. Gomez, A. W. Cohen, A. Garcia, S. Bhattacharyya, L. Shapiro, G. Dolios, R. Wang, M. P. Lisanti, et al. 2004. Perilipin A mediates the reversible binding of CGI-58 to lipid droplets in 3T3–L1 adipocytes. *J. Biol. Chem.* **279:** 42062–42071.
19. Yamaguchi, T., N. Omatsu, S. Matsushita, and T. Osumi. 2004. CGI-58 interacts with perilipin and is localized to lipid droplets. Possible involvement of CGI-58 mislocalization in Chanarin-Dorfman syndrome. *J. Biol. Chem.* **279:** 30490–30497.
20. Schweiger, M., A. Lass, R. Zimmermann, T. O. Eichmann, and R. Zechner. 2009. Neutral lipid storage disease: genetic disorders caused by mutations in adipose triglyceride lipase/PNPLA2 or CGI-58/ABHD5. *Am. J. Physiol. Endocrinol. Metab.* **297:** E289–E296.
21. Ghosh, A. K., G. Ramakrishnan, C. Chandramohan, and R. Rajasekharan. 2008. CGI-58, the causative gene for Chanarin-Dorfman syndrome, mediates acylation of lysophosphatidic acid. *J. Biol. Chem.* **283:** 24525–24533.
22. Montero-Moran, G., J. M. Caviglia, D. McMahon, A. Rothenberg, V. Subramanian, Z. Xu, S. Lara-Gonzalez, J. Storch, G. M. Carman, and D. L. Brasaemle. 2010. CGI-58/ABHD5 is a coenzyme A-dependent lysophosphatidic acid acyltransferase. *J. Lipid Res.* **51:** 709–719.
23. Crooke, R. M., M. J. Graham, K. M. Lemonidis, C. P. Whipple, S. Koo, and R. J. Perera. 2005. An apolipoprotein B antisense oligonucleotide lowers LDL cholesterol in hyperlipidemic mice without causing hepatic steatosis. *J. Lipid Res.* **46:** 872–884.
24. Brown, J. M., S. Chung, J. K. Sawyer, C. Degirolamo, H. M. Alger, T. Nguyen, X. Zhu, M. N. Duong, A. L. Wibley, R. Shah, et al. 2008. Inhibition of stearoyl-coenzyme A desaturase 1 dissociates insulin resistance and obesity from atherosclerosis. *Circulation.* **118:** 1467–1475.
25. Samuel, V. T., Z. X. Liu, X. Qu, B. D. Elder, S. Bilz, D. Befroy, A. J. Romanelli, and G. I. Shulman. 2004. Mechanism of hepatic insulin resistance in non-alcoholic fatty liver disease. *J. Biol. Chem.* **279:** 32345–32353.
26. Neschen, S., K. Morino, L. E. Hammond, D. Zhang, Z. X. Liu, A. J. Romanelli, G. W. Cline, R. L. Pongratz, X. M. Zhang, C. S. Choi, et al. 2005. Prevention of hepatic steatosis and hepatic insulin resistance in mitochondrial acyl-CoA:glycerol-sn-3-phosphate acyltransferase 1 knockout mice. *Cell Metab.* **2:** 55–65.
27. Han, X., and R. W. Gross. 2003. Global analyses of cellular lipidomes directly from crude extracts of biological samples by ESI mass spectrometry: a bridge to lipidomics. *J. Lipid Res.* **44:** 1071–1079.
28. Han, X., and R. W. Gross. 2005. Shotgun lipidomics: electrospray ionization mass spectrometric analysis and quantitation of cellular lipidomes directly from crude extracts of biological samples. *Mass Spectrom. Rev.* **24:** 367–412.
29. Yang, K., H. Cheng, R. W. Gross, and X. Han. 2009. Automated lipid identification and quantification by multidimensional mass spectrometry-based shotgun lipidomics. *Anal. Chem.* **81:** 4356–4368.
30. Lee, R. G., R. Shah, J. K. Sawyer, R. L. Hamilton, J. S. Parks, and L. L. Rudel. 2005. ACAT2 contributes cholesteryl esters to newly secreted VLDL, whereas LCAT adds cholesteryl ester to LDL in mice. *J. Lipid Res.* **46:** 1205–1212.
31. Schweiger, M., G. Schoiswohl, A. Lass, F. P. Radner, G. Haemmerle, R. Malli, W. Graier, I. Cornaciu, M. Oberer, R. Salvayre, et al. 2008. The C-terminal region of human adipose triglyceride lipase affects enzyme activity and lipid droplet binding. *J. Biol. Chem.* **283:** 17211–17220.
32. Brasaemle, D. L., and N. E. Wolins. 2006. Isolation of lipid droplets from cells by density gradient centrifugation. *Curr. Protoc. Cell Biol.* Chapter 3: Unit 3.15.
33. Yu, L., J. Li-Hawkins, R. E. Hammer, K. E. Berge, J. D. Horton, J. C. Cohen, and H. H. Hobbs. 2002. Overexpression of ABCG5 and ABCG8 promotes biliary cholesterol secretion and reduces fractional absorption of dietary cholesterol. *J. Clin. Invest.* **110:** 671–680.
34. Haemmerle, G., A. Lass, R. Zimmermann, G. Gorkiewicz, C. Meyer, J. Rozman, G. Heldmaier, R. Maier, C. Theussl, S. Eder, et al. 2006. Defective lipolysis and altered energy metabolism in mice lacking adipose triglyceride lipase. *Science.* **312:** 734–737.
35. Liang, G., J. Yang, J. D. Horton, R. E. Hammer, J. L. Goldstein, and M. S. Brown. 2002. Diminished hepatic response to fasting/refeeding and liver X receptor agonists in mice with selective deficiency of sterol regulatory element-binding protein-1c. *J. Biol. Chem.* **277:** 9520–9528.
36. Kuriyama, H., G. Liang, L. J. Engelking, J. D. Horton, J. L. Goldstein, and M. S. Brown. 2005. Compensatory increase in fatty acid synthesis in adipose tissue of mice with conditional deficiency of SCAP in liver. *Cell Metab.* **1:** 41–51.
37. Repa, J. J., G. Liang, J. Ou, Y. Bashmakov, J. M. Lobaccaro, I. Shimomura, B. Shan, M. S. Brown, J. L. Goldstein, and D. J. Mangelsdorf. 2000. Regulation of mouse sterol regulatory element-binding protein-1c gene (SREBP-1c) by oxysterol receptors, LXRalpha and LXRbeta. *Genes Dev.* **14:** 2819–2830.
38. Bauman, D. R., A. D. Bitmansour, J. G. McDonald, B. M. Thompson, G. Liang, and D. W. Russell. 2009. 25-Hydroxycholesterol secreted by macrophages in response to Toll-like receptor activation suppresses immunoglobulin A production. *Proc. Natl. Acad. Sci. USA.* **106:** 16764–16769.
39. Gruber, A., I. Cornaciu, A. Lass, M. Schweiger, M. Poeschl, C. Eder, M. Kumari, G. Schoiswohl, H. Wolinski, S. D. Kohlwein, et al. 2010. The N-terminal region of comparative gene identification-58 (CGI-58) is important for lipid droplet binding and activation of adipose triglyceride lipase. *J. Biol. Chem.* **285:** 12289–12298.
40. Houtkooper, R. H., and F. M. Vaz. 2008. Cardiolipin, the heart of mitochondrial metabolism. *Cell. Mol. Life Sci.* **65:** 2493–2506.
41. Numata, M., H. W. Chu, A. Dakhama, and D. R. Voelker. 2010. Pulmonary surfactant phosphatidylglycerol inhibits respiratory syncytial virus-induced inflammation and infection. *Proc. Natl. Acad. Sci. USA.* **107:** 320–325.
42. Kim, J. K., O. Gavrilova, Y. Chen, M. L. Reitman, and G. I. Shulman. 2000. Mechanism of insulin resistance in A-ZIP/F-1 fatless mice. *J. Biol. Chem.* **275:** 8456–8460.
43. Kim, J. K., Y. J. Kim, J. J. Fillmore, Y. Chen, I. Moore, J. Lee, M. Yuan, Z. W. Li, M. Karin, P. Perret, et al. 2001. Prevention of fat-induced insulin resistance by salicylate. *J. Clin. Invest.* **108:** 437–446.
44. Gavrilova, O., B. Marcus-Samuels, D. Graham, J. K. Kim, G. I. Shulman, A. L. Castle, C. Vinson, M. Eckhaus, and M. L. Reitman. 2000. Surgical implantation of adipose tissue reverses diabetes in lipoatrophic mice. *J. Clin. Invest.* **105:** 271–278.
45. Samuel, V. T., Z. X. Liu, A. Wang, S. A. Beddow, J. G. Geisler, M. Kahn, X. M. Zhang, B. P. Monia, S. Bhanot, and G. I. Shulman. 2007. Inhibition of protein kinase Cepsilon prevents hepatic insulin resistance in nonalcoholic fatty liver disease. *J. Clin. Invest.* **117:** 739–745.
46. Erion, D. M., and G. I. Shulman. 2010. Diacylglycerol-mediated insulin resistance. *Nat. Med.* **16:** 400–402.
47. Listenberger, L. L., X. Han, S. E. Lewis, S. Cases, R. V. Farese, Jr., D. S. Ory, and J. E. Schaffer. 2003. Triglyceride accumulation protects against fatty acid-induced lipotoxicity. *Proc. Natl. Acad. Sci. USA.* **100:** 3077–3082.